Measurements and Predictions of Endwall Heat Transfer in Two High Pressure Turbines

M.A. Hilditch, G.C. Smith and K.S. Chana
The Sir Frank Whittle Building
DERA Farnborough
Farnborough
Hants
GU14 0LX

Summary
Accurate predictions of turbine heat transfer rates are needed to reduce the overall costs and risks of developing an efficient cooling system and to improve predictions of turbine life. 3D Navier Stokes codes are commonly used to predict the aerodynamic flowfield, but their use for heat transfer calculations is not so well established. This paper describes heat transfer predictions for the endwalls of two high pressure nozzle guide vanes using a typical Navier Stokes code and Baldwin Lomax turbulence model. The results are compared with experimental data and other published calculations and can be explained in terms of the endwall secondary flows.

Introduction
One of the most difficult problems facing the turbine designer is that of predicting the heat transfer rates and hence metal temperatures of the components. The metal temperature affects the life of a component, and the overall thermodynamic cycle efficiency of the engine. An improvement in cycle efficiency comes not just from allowing an increase in the turbine entry temperature (TET), but from a reduction in cooling flows made possible by more accurate temperature predictions. Current design methods are based largely on crude empirical analysis and extensive thermal paint tests. Any improvement in design procedures through the use of computational fluid dynamics (CFD) would be of great benefit to both the final design and the development process.

This work has been aimed at evaluating the performance of CFD to predict heat transfer to high pressure (HP) nozzle guide vanes (NGV). This numerical analysis has used the TRANSCode structured solver CFD code available to the DERA Turbomachinery group. Two NGVs have been studied, MT1 and the high rim speed turbine (HRST). Heat transfer measurements are available for both these NGVs, as well as other experimental data including flow visualisation and measurements of total pressure at exit.

Smith et al (2001) describe work at DERA to predict Nusselt number profiles on the turbine aerofoils. The Nusselt number distribution on an aerofoil can be largely regarded as two dimensional, whereas endwall heat transfer predictions provide a severe test for 3D viscous flow analysis as the heat transfer is strongly affected by the secondary flows present in the turbine passage. The aim of this study was to evaluate the quality of heat transfer predictions available from a typical Navier Stokes code and algebraic turbulence model. The code in question has been extensively used for aerodynamic analysis of turbomachines, but had not been benchmarked against turbine heat transfer data in its present form and using modern computer workstations.

Paper presented at the RTO AVT Symposium on "Advanced Flow Management: Part B – Heat Transfer and Cooling in Propulsion and Power Systems", held in Loen, Norway, 7-11 May 2001, and published in RTO-MP-069(I).

Report Documentation Page

Form Approved
OMB No. 0704-0188

1. REPORT DATE	2. REPORT TYPE	3. DATES COVERED
00 MAR 2003	**N/A**	**-**

4. TITLE AND SUBTITLE	5a. CONTRACT NUMBER
Measurements and Predictions of Endwall Heat Transfer in Two High Pressure Turbines	5b. GRANT NUMBER
	5c. PROGRAM ELEMENT NUMBER
6. AUTHOR(S)	5d. PROJECT NUMBER
	5e. TASK NUMBER
	5f. WORK UNIT NUMBER
7. PERFORMING ORGANIZATION NAME(S) AND ADDRESS(ES) **NATO Research and Technology Organisation BP 25, 7 Rue Ancelle, F-92201 Neuilly-Sue-Seine Cedex, France**	8. PERFORMING ORGANIZATION REPORT NUMBER
9. SPONSORING/MONITORING AGENCY NAME(S) AND ADDRESS(ES)	10. SPONSOR/MONITOR'S ACRONYM(S)
	11. SPONSOR/MONITOR'S REPORT NUMBER(S)

12. DISTRIBUTION/AVAILABILITY STATEMENT
Approved for public release, distribution unlimited

13. SUPPLEMENTARY NOTES
Also see ADM001490, presented at RTO Applied Vehicle Technology Panel (AVT)Symposium held in Leon, Norway on 7-11 May 2001, The original document contains color images.

14. ABSTRACT

15. SUBJECT TERMS

16. SECURITY CLASSIFICATION OF:			17. LIMITATION OF ABSTRACT	18. NUMBER OF PAGES	19a. NAME OF RESPONSIBLE PERSON
a. REPORT	b. ABSTRACT	c. THIS PAGE			
unclassified	**unclassified**	**unclassified**	**UU**	**14**	

Standard Form 298 (Rev. 8-98)
Prescribed by ANSI Std Z39-18

Secondary flows in NGVs

The secondary flow in a vane passage is caused by two main mechanisms, the cross passage pressure gradient and the horseshoe vortex (see Figure 1). Their relative strength and interaction depend on the geometry of the blade and the inlet flowfield. Consequently, some detailed observations described in the literature are not applicable in all cases. A general description of the flow field is given by Graziani et al (1980).

Strong pressure gradients exist across the passage due to the turning and acceleration of the mainstream flow. The boundary layer within the passage is driven from the pressure surface towards the suction surface and over turns when it encounters the suction surface, forming the passage vortex. The horseshoe vortex is formed when the inlet endwall boundary layer rolls up at the leading edge of the aerofoil. It is wrapped around the leading edge forming two legs, one in each passage. The pressure surface leg moves across the passage towards the suction surface because of the pressure gradient and may become part of the passage vortex. The suction surface leg remains close to the vane as it is swept downstream.

The path of the horseshoe vortex forms a separation line across the endwall. Upstream of the separation line the inlet boundary layer is skewed by the pressure gradient and flows towards the suction surface, along with the pressure surface leg of the horseshoe vortex. Downstream of the separation line a new boundary layer forms on the endwall. This is also moved towards the suction surface by the pressure gradient.

In an annular blade ring, where the exit flow is not axial, the tangential flow sets up a radial pressure gradient with higher pressure on the casing. This pushes the hub secondary flows at exit from the blade row on to the endwall and causes the secondary flows on the casing to move away from the wall.

MT1 and HRST test cases

Heat transfer measurements were made on the two NGVs in the Isentropic Light Piston Facility (ILPF) at DERA Pyestock. HRST was tested as an annular cascade in 1987 (Chana, 1994). Later the ILPF was upgraded to incorporate the MT1 turbine as a rotating stage (Hilditch et al, 1994). Static pressure and heat transfer measurements, both steady and unsteady on both NGV and rotor blade have been reported previously (Hilditch et al, 1995 and Hilditch et al, 1998) as have measurements of unsteady total temperature. Measurements have also been made on the vane alone in the ILPF (Harvey et al, 1998).

The ILPF is a short duration wind tunnel capable of representing the conditions found in an engine for approximately half a second. The operating conditions of the two turbines as tested in the ILPF are listed in Table 1.

	MT1	HRST
NGV exit Mach number at hub	1.034	1.14
NGV inlet total temperature (K)	444.4	440.0
NGV inlet total pressure (Pa)	461500	495430
Exit swirl angle (mid-height)	74.4°	75.4°
Exit Reynolds number	2.6×10^6	3.4×10^6
Aspect ratio	0.53	0.52
NGV chord (mm)	70.1	74.5
Inlet turbulence level	6%	6%

Table 1: MT1 and HRST NGV operating parameters

The heat transfer measurements described in this report were made by mounting thin film heat transfer gauges on vanes manufactured from machinable glass ceramic. The thin film gauges measure the surface temperature of the model and by assuming one-dimensional conduction of heat into the model, the heat transfer rate can be established. This was done using an electrical analogue that exactly models the transient conduction equation and produces an output directly proportional to heat transfer rate (Oldfield et al, 1978).

The heat transfer measurements are presented as Nusselt number (*Nu*), where

$$Nu = \frac{\dot{q}C}{(T_0 - T_w)k} \qquad (1)$$

and $\dot{q}$ is the measured heat transfer rate, C the vane true chord, T_0 the measured total temperature of gas at inlet, T_w the measured surface temperature and *k* is gas conductivity evaluated as follows:

$$k = 0.0047 + 7.0e^{-5}T_0 \qquad (2)$$

The experimental uncertainties associated with these heat transfer measurements have been analysed and the Nusselt number uncertainty is estimated to be +/-8%.

TRANSCode calculations

TRANSCode (Calvert et al, 1997) is a 3D viscous flow program developed at DERA from the BTOB3D code written by Dawes (1988). It is extensively used by the Turbomachinery group at DERA Pyestock for the aerodynamic design and analysis of transonic fans, core compressors and turbines. The latest version of the code has options for a generalised H-mesh and Spalart Allmaras turbulence model, but for these calculations (unless otherwise stated) a single body fitted sheared H mesh and a Baldwin Lomax turbulence model were used. The flow on the endwalls was set to be turbulent at all locations, while the flow on the aerofoils was transitional.

Heat transfer calculations require the cell spacing near the wall to be sufficiently small so as to resolve the viscous sub-layer. If this cannot be achieved TRANScode employs wall functions to make corrections to both the shear stress and heat flux at the wall. This study set out to achieve y+ values approaching 1, by packing cells near the wall, but still maintaining an acceptable grid density in mid-passage. For HRST the grid was optimised to give the minimim y+ values on the aerofoil and larger values were allowed on the endwalls. Other constraints such as cell skew and aspect ratio resulted in grids of different size and cell spacing for the two turbines, as shown in Table 2.

	Number of radial and spanwise cells	Maximum cell size/wall cell size	Typical endwall y+ values	Total number of nodes
MT1	73	800	2	890,000
HRST	73	50	10	634,000

Table 2: Grid details

A grid dependency study and other details of the calculation are reported by Smith et al, (2001). For y+ values less than 5, the wall functions had no effect and further reduction in y+ values produced negligible differences in the predicted heat transfer values. The y+ values for HRST endwalls are aproximately 10, so the wall functions will apply a small correction, but in general the grid differences for the two test cases are not considered to influence the quality of the predictions.

Predictions of MT1

The static pressure distributions predicted for the endwalls were in excellent agreement with experiment and are not shown. Figure 2 shows the Nusselt number prediction for the MT1 hub and casing, and the corresponding experimental data are plotted in Figure 3. The crosses show the measurement locations. The measurement devices themselves were not point locations, but thin film gauges approximately 4 mm long and 0.5 mm wide. Consequently, each measurement is an average of the heat transfer over the area of the thin film gauge and this should be considered when comparing experimental and CFD results.

The predicted Nusselt number contours on the hub and casing agree with the expected flow patterns described earlier. The black lines are particle paths showing the formation and movement of the horseshoe vortex. The heat flux levels are low at inlet and increase through the passage as would be expected in accelerating flow. The contour pattern broadly follows the path of the pressure surface leg of the horseshoe vortex from the leading edge of the pressure surface towards the trailing edge of the suction surface. At inlet the Nusselt numbers are higher near the pressure surface than in mid-passage. This is consistent with the inlet boundary layer being rolled up into the horseshoe vortex and a new (thin) boundary layer forming. A region of low heat transfer is predicted near the suction surface trailing edge on the hub and to a lesser extent on the casing. This is thought to be caused by the migration of low momentum fluid from the endwall boundary layer and the horseshoe vortex on to these regions of the blade.

The discontinuity seen in the predicted Nusselt number near the pressure surface at 75% axial chord is caused by the implementation of the Baldwin Lomax turbulence model. Figure 4 is a plot of the parameter Ymax (Baldwin and Lomax, 1978) which is used in the calculation of the turbulent viscosity. At several locations including 75% axial chord (J≈90) it can be seen to suddenly change level and then recover to the previous value. This switching between the two values of Ymax is a known problem of this type of model where the history of the turbulent flow is not accounted for. As a check on the CFD code the calculation for MT1 was repeated using the Spalart Allmaras turbulence mode, which overcomes this problem by modelling the transport of turbulence. The results for the hub are shown in Figure 5 and are very similar to those with the Baldwin Lowmax turbulence model, but show a continuous zone of high heat transfer near the pressure surface trailing edge. All other predictions in this paper use the Baldwin Lomax turbulence model, and display a discontinuity in the heat transfer contours, which should be ignored.

Comparison with the experimental results show that the predicted and measured Nusselt numbers at inlet on the hub are in good agreement, while on the casing the predicted Nusselt numbers are higher than measured. Moving downstream the value of the prediction for both endwalls increases more quickly than the experimental measurements, so towards the rear of the passage the predicted results are becoming progressively higher than the experiment. It must be remembered that the measurements are averaged over the area of the thin film gauge (4 x 0.5 mm) and this would tend to smooth out the peak values. The highest Nusselt numbers measured on the hub were near the pressure surface trailing edge, but they are less than those predicted in this region. Measurements on the casing show less change in heat transfer than on the hub, while the predictions show a more pronounced area of high heat transfer a little distance away from the pressure surface trailing edge.

The regions of high Nusselt number predicted on the crown of the suction surface for both endwalls are not present in the experimental results. This may be because insufficient experimental readings were taken to allow the effect to be resolved. The region of decreasing heat transfer predicted near the suction surface trailing edge is repeated in the experimental results on the hub, but confined to two gauges only on the casing.

Flow visualisation experiments were undertaken in the ILPF using a mixture of silicone oil and paraffin coloured with fluorescent dye. Before a run the endwall upstream of the leading edges was painted red, the aerofoils painted yellow and the blade passages on the hub and casing were painted green. The vanes were then replaced in the facility and the tunnel was run. They were then removed to be examined and photographed.

The results are shown in Figures 6 and 7. (The area between the red stripes on Figure 7 is yellow, although it looks green in the photograph). The red dye initially upstream of the blade row is swept towards the suction surface at the inlet to the blade row. So fluid from the inlet boundary layer does not reach the pressure surface half of the passage and a new boundary layer must be growing here. Further downstream red dye from the inlet boundary layer and green dye from the end wall area are swept up onto the suction surface. This migration towards mid span is more pronounced at the casing than the hub end of the blade; this is consistent with the effects of the radial pressure gradient.

The prediction using the Baldwin Lomax turbulence model for the aerofoil suction surface (Figure 8) shows two regions of reduced Nusselt number near the endwalls towards the trailing edge. This is where the endwall boundary layer washes up the blade surface. The reduced heat transfer towards the trailing edge near the hub can be explained by the radial pressure gradient keeping the low momentum secondary flows close to the hub endwall, whereas the casing secondary flows are moved towards mid-span.

Nusselt number calculations for MT1 NGV have also been reported by Harvey et al (1998) at three operating conditions (of which the high Mach number case best matches the experimental conditions in Table 1). The calculations were performed using a 3D steady, viscous, finite volume, pressure correction method and one priority was to keep computational run times sufficiently low for engine design purposes. This was achieved in part by the use of coarse grids (140,000 points) and wall functions. The results were similar to those presented here in both pattern and level, with high heat transfer seen near the pressure surface trailing edge and suction surface crown.

Spencer et al (1995) have reported full coverage liquid crystal measurements over the endwalls of another high pressure turbine. Their results again show heat transfer coefficients which generally increase as the flow accelerates through the passage, highest heat transfer near the pressure surface trailing edge and a zone of low heat transfer near the suction surface trailing edge. A region of very high heat transfer was also seen on the suction surface near the leading edge. Such a feature was seen in the current predictions and those of Harvey, but was not resolved by the thin film gauge measurements. High heat transfer in this region can be explained by the accelerating flow and scouring action of the horseshoe vortex.

In general the predictions obtained from TRANSCode were encouraging. The heat transfer contours are consistent with the expected flow regime in that the predicted contour patterns appeared to match the path of the horseshoe vortex. Also, a region of high heat transfer is seen close to the pressure surface. Flow visualisation has shown that the inlet boundary layer is swept away from this region and a new, thin, boundary layer must be growing. On the suction surface regions of low heat transfer were predicted where flow visualisation has shown the boundary layer to wash up the surface.

Predictions of HRST

Predictions of the endwall static pressure again showed excellent agreement with measurements, and are not shown. The NGV exit total pressure field was measured on a plane 20% of an axial chord downstream of the trailing edge, Figure 9. The corresponding prediction is shown in Figure 10. The two are in good agreement, especially in terms of wake depth and thickness. There is

some discrepancy between measurement and CFD in the angle of the wake near the endwalls. This may be due to differences in secondary flow location and strength, resulting in a change to the over/under turning profile.

The measured Nusselt number distribution for the hub and casing endwalls of HRST are shown in Figure 11. The corresponding predictions are plotted in Figure 12 and are similar in form to those for MT1. Again there is a spurious discontinuity in the Nusselt number at approximately 75% axial chord, resulting from the implementation of the Baldwin Lomax turbulence model. There is a “v-shaped” region of low heat transfer extending into the passage. Close to the pressure surface the heat transfer increases with distance, reaching a peak at 60% axial chord. On the suction surface there is a region of very high heat transfer near the leading edge that extends over much of the suction surface, but close to the suction surface trailing edge the heat transfer is again much reduced.

The measured heat transfer distributions are very similar for both hub and casing. The Nusselt number is low at inlet and increases as the flow accelerates. The highest Nusselt numbers (>3600) are seen near the pressure surface trailing edges and on the crown of the suction surface, whereas a region of low Nusselt number is seen close to the suction surface trailing edge on both endwalls. In general the predicted Nusselt numbers are higher than the measurements. The best agreement is found near the pressure surface trailing edge, where the maximum values are found for both predictions and measurements. As with MT1 the measured contour patterns are much less detailed than the predictions and there is no evidence in the experiment of a region of high heat transfer near the early suction surface. One reason for this has to be the limited number of measurement locations and the shape of the sensors which averages the heat transfer over a 4 x 0.5 mm strip.

Predictions for this HRST dataset have also been reported by Boyle and Jackson (1995). They used two codes, the finite volume code TRAF3D with a Baldwin Lomax turbulence model and the finite difference code RVC3D with a choice of Chima’s modified Baldwin-Lomax turbulence model and the Cebeci-Smith turbulence model. The endwall Nusselt number for the TRAF3D code with Baldwin–Lomax turbulence model is very similar to the results presented here in both pattern and level (Figure 13). The Nusselt number contours predicted by the other code and turbulence models were different in shape and so choosing the best prediction was not easy, especially as the level of agreement between the three predictions and the experiment varied around the blade. Boyle and Jackson concluded that the Cebeci-Smith turbulence model gave the best agreement with measurements, but still overpredicted the peak heat transfer.

Predictions using the RVC3D code for a large number of test cases were reported by Boyle and Lucci (1996). Again a number of algebraic turbulence models were used and in general the peak heat transfer was predicted to be higher than measured. In most cases, high heat transfer was predicted near the crown of the suction surface, but this level of detail could not be resolved by the experimental measurements.

Conclusions

Predictions of endwall heat transfer have been made using a 3D Navier stokes code for two high pressure turbine vanes. The results show good qualitative agreement with the expected secondary flow features, however the agreement with experimental data in both pattern and level was not so good. The differences in pattern are due partly to the limited number of experimental data points and size of the thin film gauge over which the results will have been averaged. The differences in level were expected as other similar codes have also been reported as overpredicting endwall heat transfer to a similar extent (approximately 20%).

The difficulties in calculating endwall heat transfer rates stem from the need to model the detailed flow field in the boundary layer in a way that is computationally efficient and provides a good model of the flow physics. These results demonstrate what is possible from a modern CFD code using a Baldwin Lomax turbulence model. There is still much room for improvement, but how this will be achieved is uncertain. Changes in turbulence and transition modelling are obvious areas to explore, but there are many possible approaches all involving simplification and compromise. These must be evaluated thoroughly, as approaches that accurately model the transport of heat within the boundary layer on a flat plate are not necessarily applicable to a turbine blade.

References

Baldwin, B.S. and Lomax, H., 1978, "Thin-layer approximation and algebraic model for separated turbulent flows", AIAA Paper 78-257

Boyle, R.J. and Lucci, B.L., 1996, "Predicted turbine heat transfer for a range of test conditions", ASME paper 96-GT-304.

Boyle, R.J. and Jackson, R., 1995, "Heat transfer predictions for two turbine nozzle geometries at high Reynolds and Mach numbers", ASME paper 95-GT-104.

Calvert, W.J., Stapleton, A.W., Emmerson, P.R., Buchanan, C.R. and Nott, C.M., 1997, "Evaluation of a 3D viscous code for turbomachinery flows", ASME paper 97-GT-078.

Chana, K.S., 1994, "Heat transfer and aerodynamics of a high rim speed turbine nozzle guide vane with profiled end walls", ASME paper 94-GT-123.

Dawes, W.N., 1988, "Development of a 3D Navier-Stokes solver for application to all types of turbomachinery", ASME paper 88-GT-70.

Graziani, R.A. Blair, M.F., Taylor, J.R. and Mayle, R.E., 1980, "An experimental study of end wall and airfoil surface heat transfer in a large scale turbine blade cascade", *ASME Journal of Engineering for Power*, Vol 102, No 2, Apr. 1980, pp. 257-267

Harvey, N.W., Rose, M.G., Coupland, J and Jones, T.V., 1998, "Measurement and calculation of nozzle guide vane end wall heat transfer", ASME paper 98-GT-66

Hilditch, M.A., Fowler, A., Jones, T.V., Chana, K.S., Oldfield, M.L.G., Ainsworth, R.W., Hogg, S.I., Anderson, S,J, and Smith, G.C., 1994, "Installation of a turbine stage in the Pyestock Isentropic Light Piston Facility", ASME paper 94-GT-277

Hilditch, M A, Smith, G.C., Anderson, S.J. and Chana, K.S., Jones, T.V., Ainsworth, R.W. and Oldfield, M.L.G., 1995, "Unsteady measurements in an axial flow turbine", AGARD CP571, *Loss mechanisms and unsteady flows in turbomachines*

Hilditch M A., Smith, G C and Singh, U K, 1998, "Unsteady flow in a single stage turbine", ASME paper 98-GT-531

Oldfield, M.L.G., Jones, T.V. and Schultz, D.L., 1978, "On line computer for transient turbine cascade instrumentation in transient tunnels", IEEE Trans. Aerospace Electronic Systems AES-14 (5).

Smith, G.C., Hilditch, M.A. and Wood, N.B., 2001, "Heat transfer computations for high pressure turbines", ASME paper 2001-GT-0172

Spencer, M.D., Lock, G.D., Jones, T.V. and Harvey, N.W., 1995, “Endwall heat transfer and aerodynamic measurements in an annular cascade of nozzle guide vanes”, ASME paper 95-GT-356

Acknowledgements
This work was funded by the UK Department of Trade and Industry (CARAD) and Ministry of Defence (ARP26c).

Figures

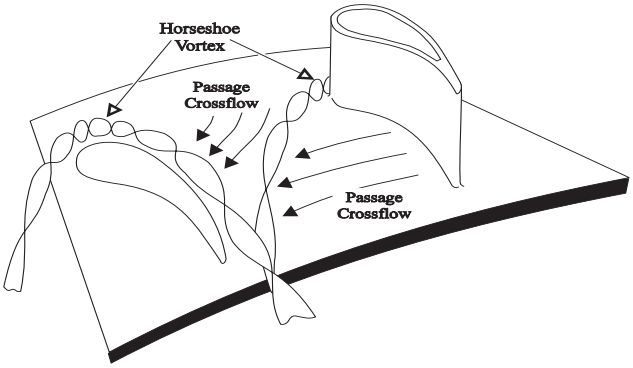

Figure 1; Secondary flow in the NGV passage

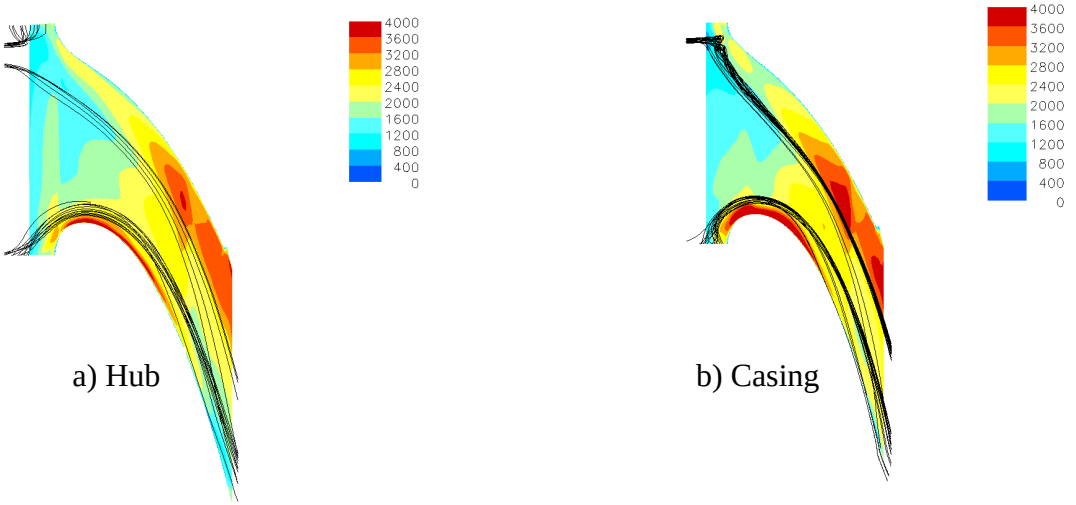

Figure 2; Predicted endwall Nusselt number for MT1

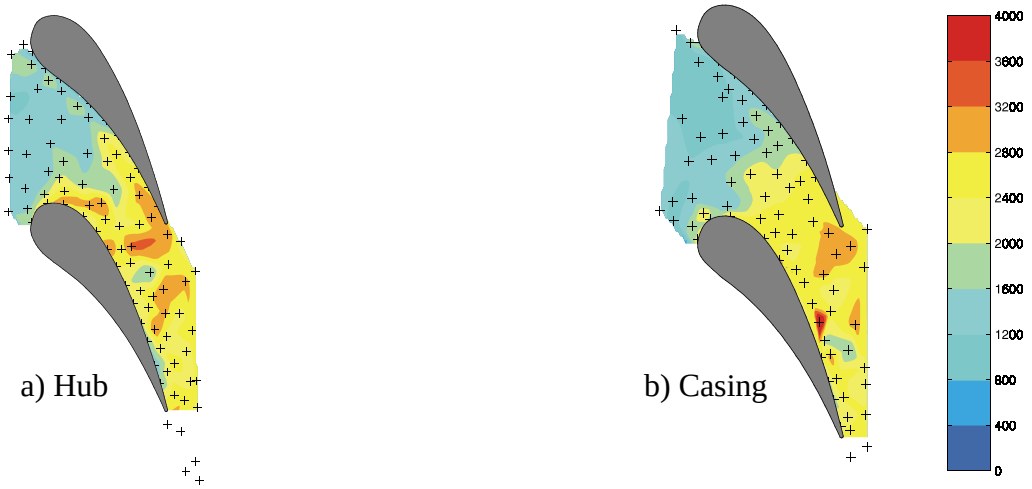

Figure 3; Measured endwall Nusselt number for MT1

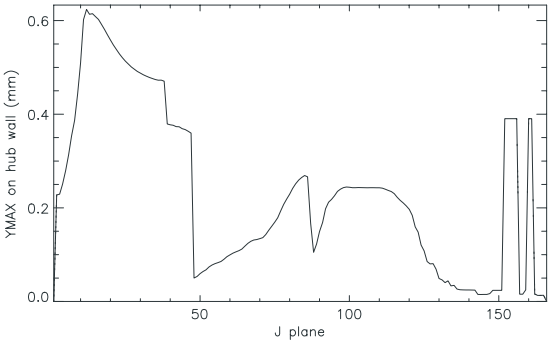

Figure 4; Distribution of Ymax for the Baldwin Lomax solution

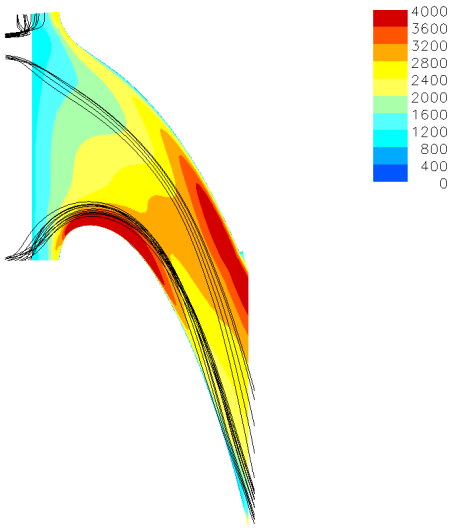

Figure 5; Predicted hub Nusselt number for MT1 using the Spalart Allmaras turbulence model

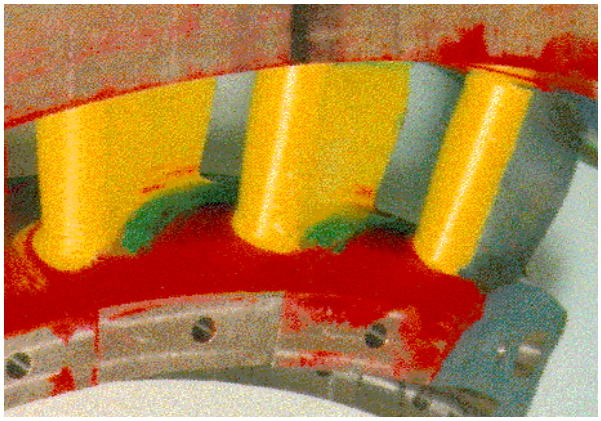

Figure 6; Flow visualisation of the MT1 hub

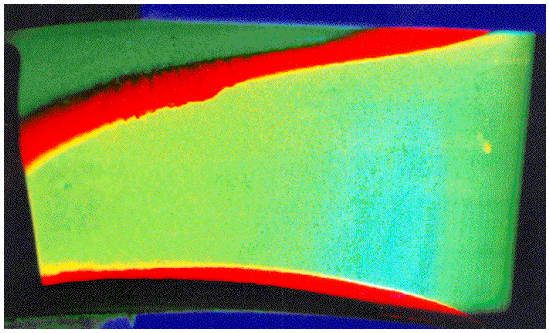

Figure 7; Flow visualisation of the MT1 suction surface

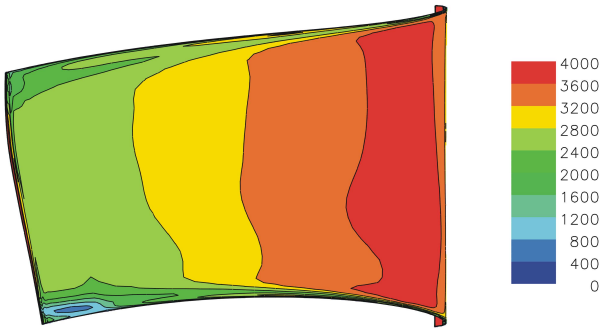

Figure 8; Predicted Nusselt number for the MT1 suction surface

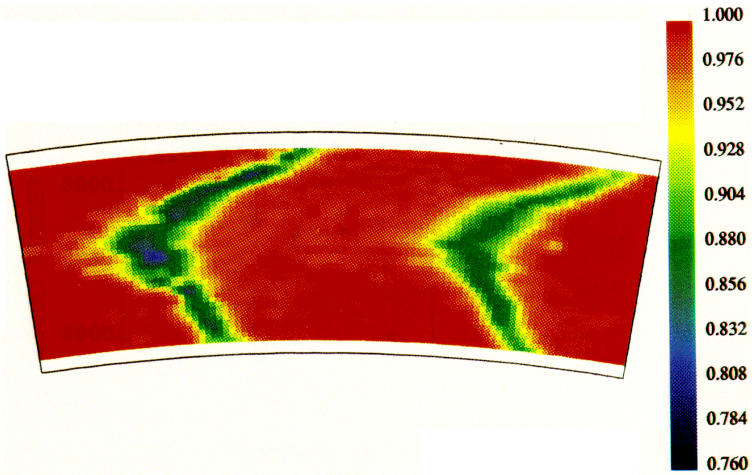

Figure 9; Measured total pressure ratio at 120% axial chord

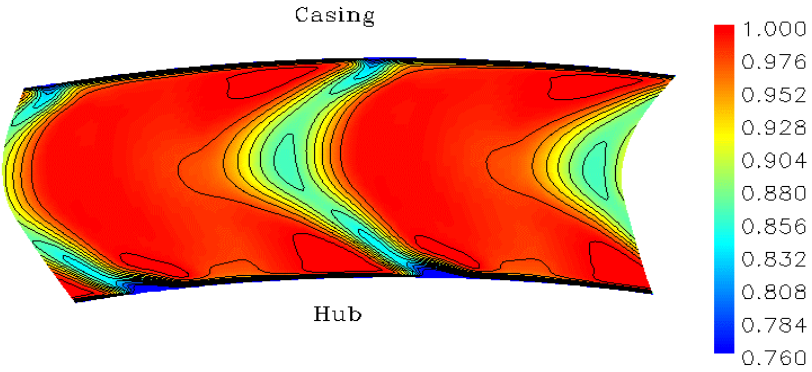

Figure 10; Predicted total pressure ratio at 120% axial chord

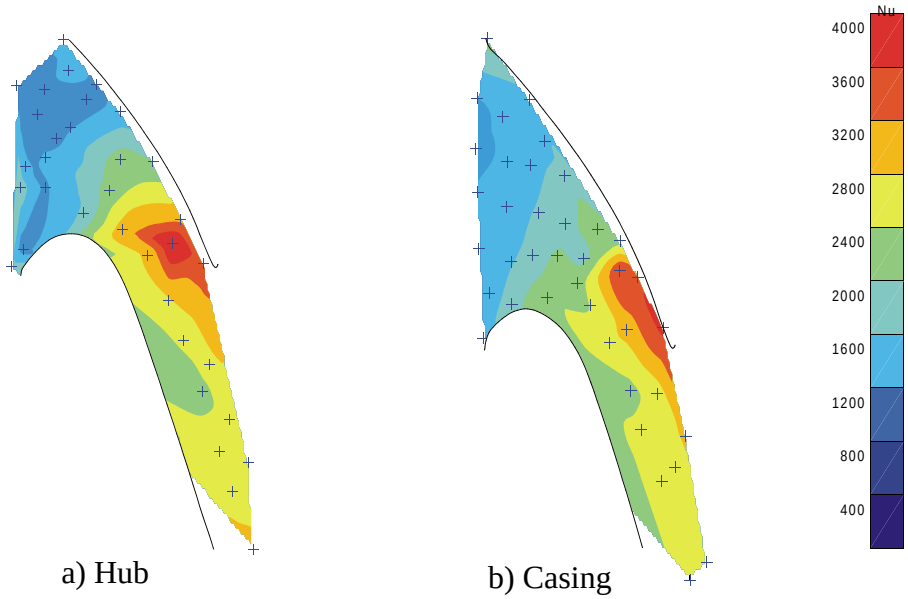

Figure 11; Measured endwall Nusselt number for HRST

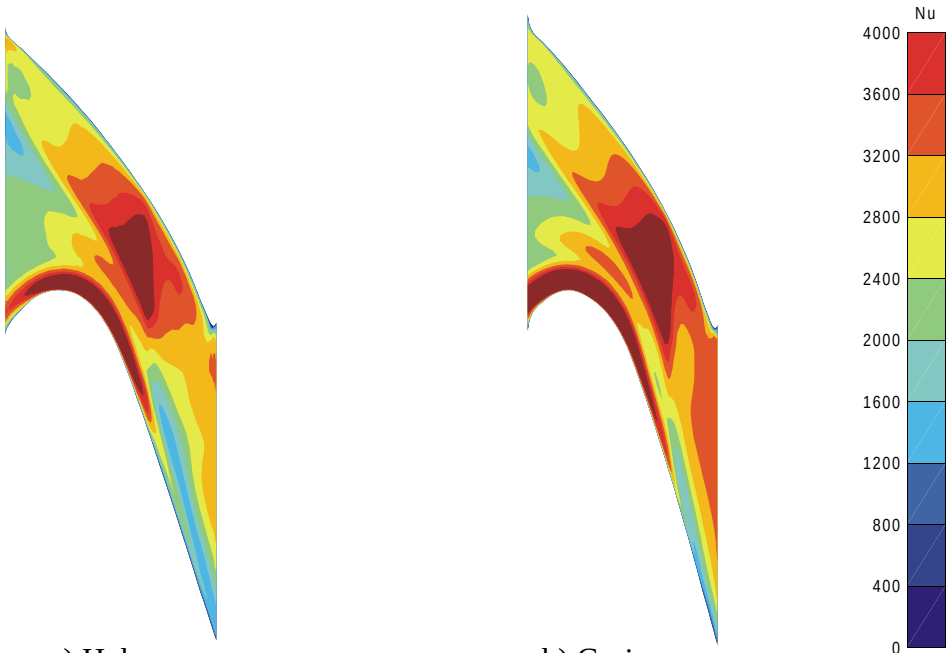

a) Hub b) Casing

Figure 12; Predicted endwall Nusselt number for HRST

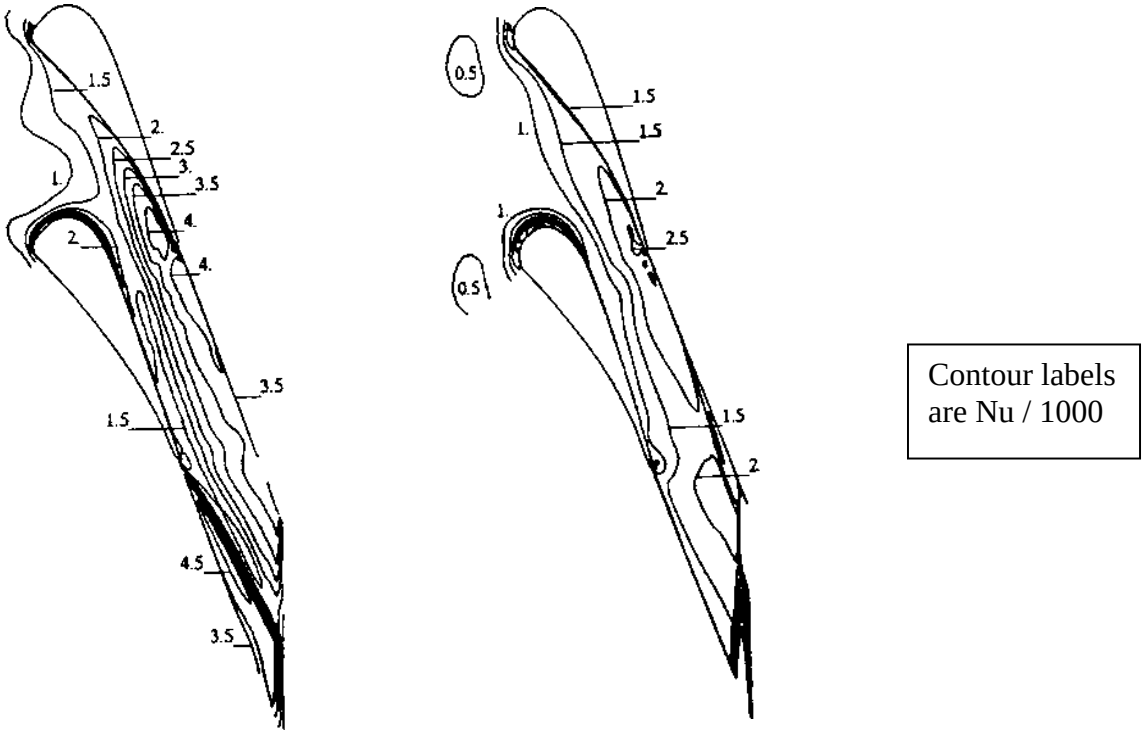

a) Hub b) Casing

Figure 13; Endwall heat transfer for HRST reproduced from Boyle and Jackson (1995)

Paper Number: 37

Name of Discusser: B.H. Weyer, DLR Cologne

Question:

1 Did you consider BL-transition with your calculations?

2 In a highly, 3-D flow it is difficult to define the reference temperature for the heat transfer prediction. What is your definition?

Answer:

1 For these calculations the endwall was set as turbulent. We felt that the strong secondary flows seen on the endwalls meant they were mostly turbulent.

3 For the reference temperature we used the inlet total temperature in both the experiment and predicted case.

This page has been deliberately left blank

Page intentionnellement blanche